

Improved gray matter surface based spatial statistics in neuroimaging studies

Prasanna Parvathaneni^{1*}, Ilwoo Lyu², Yuankai Huo¹, Baxter P. Rogers³, Kurt G. Schilling³, Vishwesh Nath², Justin A. Blaber¹, Allison E. Hainline⁴, Adam W. Anderson³, Neil D. Woodward⁵, Bennett A. Landman^{1,2,3,5}

¹Electrical Engineering, Vanderbilt University, Nashville, TN, USA

²Computer Science, Vanderbilt University, Nashville, TN, USA

³Vanderbilt University Institute of Imaging Science, Vanderbilt University, Nashville, TN, USA

⁴Biostatistics, Vanderbilt University, Nashville, TN, USA

⁵Department of Psychiatry and Behavioral Sciences, Vanderbilt University, Nashville, TN, USA

*Corresponding author

E-mail: Prasanna.Parvathaneni@Vanderbilt.edu (PP)

Abstract

Neuroimaging often involves acquiring high-resolution anatomical images along with other low-resolution image modalities, like diffusion and functional magnetic resonance imaging. Performing gray matter statistics with low-resolution image modalities is a challenge due to registration artifacts and partial volume effects. Gray matter surface based spatial statistics (GS-BSS) has been shown to provide higher sensitivity using gray matter surfaces compared to that of skeletonization approach of gray matter based spatial statistics which is adapted from tract based spatial statistics in diffusion studies. In this study, we improve upon GS-BSS incorporating neurite orientation dispersion and density imaging (NODDI) based search (denoted N-GSBSS) by 1) enhancing metrics mapping from native space, 2) incorporating maximum orientation dispersion index (ODI) search along surface normal, and 3) proposing applicability to other modalities, such as functional MRI (fMRI). We evaluated the performance of N-GSBSS against three baseline pipelines: volume-based registration, FreeSurfer's surface registration and ciftify pipeline for fMRI and simulation studies. First, qualitative mean ODI results are shown for N-GSBSS with and without NODDI based search in comparison with ciftify pipeline. Second, we conducted one-sample t-tests on working memory activations in fMRI to show that the proposed method can aid in the analysis of low resolution fMRI data. Finally we performed a sensitivity test in a simulation study by varying percentage change of intensity values within a region of interest in gray matter probability maps. N-GSBSS showed higher sensitivity in the simulation test compared to the other methods capturing difference between the groups starting at 10 percent change in the intensity values. The computational time of N-GSBSS is 68 times faster than that of traditional surface-based or 86 times faster than that of ciftify pipeline analysis.

38 **Keywords:** NODDI, AMICO, Microstructure imaging, spatial statistics, Gray matter, Advanced DW-
39 MRI, functional MRI, GBSS, TBSS, GS-BSS, Ciftify

40 1. Introduction

41 Gray matter (GM) in the cerebral cortex is key to many sensory, cognitive, and motor functions of the
42 brain. Detecting cortical alterations with neuropathologic conditions could provide potential
43 biomarkers to facilitate early diagnosis and assessment of disease severity. In recent years, the
44 development of neuroimaging techniques, such as high-resolution magnetic resonance imaging (MRI),
45 functional magnetic resonance imaging (fMRI), diffusion weighted magnetic resonance imaging
46 (dMRI), positron emission tomography (PET) or single photon emission computed tomography
47 (SPECT), have promoted the identification of structural and functional characteristics of the
48 developing brain and underlying mental disorders [1-7]. An increasing number of studies have shown
49 structural and functional gray matter changes in clinical applications - e.g., amyotrophic lateral
50 sclerosis [8], schizophrenia and bipolar disorder [9, 10], age related effects [11], attention deficit
51 hyperactivity disorder [12], and Alzheimer’s disease [13]. While T1 images can be acquired at high
52 resolution (e.g., 1 mm isotropic), clinical imaging in other modalities (such as dMRI and fMRI) are
53 constrained by imaging and physiological factors leading to lower resolution (2-3 mm isotropic). As
54 the cortex is about 1.6 – 4.5 mm thick [14-16] within the gray matter tissue region between white and
55 pial surfaces, significant challenges arise with cross subject analysis involving registration artifacts and
56 partial volume effects [17]. The individual cortical anatomy may not be sufficiently aligned after non-
57 rigid volumetric registration since it is quite challenging to incorporate spatial coherence in the
58 volumetric images (see Fig 1-a). In particular, volumetric smoothing potentially introduces partial
59 volume effects since the cortical structure is thinner, as seen in Fig 1-b. This issue was successfully
60 addressed in WM using tract based spatial statistics (TBSS) [18], which has proven to be a popular
61 technique for performing voxel-wise statistical analysis with improved sensitivity and interpretability
62 of analysis of multi-subject diffusion imaging studies in white matter (WM) [19-23]. Gray matter
63 based spatial statistics (GBSS) adapted the TBSS framework for GM using neurite orientation
64 dispersion and density imaging (NODDI) [11] to perform voxel-wise statistical analysis on GM
65 microstructure in diffusion studies. GBSS employs skeletonized cortical ribbon to capture diffusion
66 metrics along its trajectories. However, this approach could yield low sensitivity to the cross sectional
67 differences around the cortical sulci since GM skeletonization is extracted only along highly
68 overlapping regions. To overcome this issue, we proposed an alternate approach known as gray matter
69 surface based spatial statistics (GS-BSS) [24] that employs a cortical surface to increase the number of
70 highly probable GM vertices that closely follow the cortex (Fig 1b).

71

Fig 1: (a) Non-rigid image registration of GM probability maps of three subjects. Each color box highlights the corresponding region of interest. Right column shows detailed differences in cortical folding patterns across the subjects. (b) Skeletonized GM (red) and cortical central surface (yellow) are overlaid on T1 image. GM central surface closely follows the cortical structure compared to that of skeletonized GM approach. Two examples are highlighted in blue and green boxes where GM cortical surface closely follows the cortical structure compared to the volumetric based GM skeletonization approach. Darker regions on T1 indicate GM and lighter regions represent WM.

72

73 In volumetric neuroimaging analyses, spatial smoothing is generally performed to improve image
74 alignment and statistical sensitivity, at the cost of specificity of the underlying region of interest [25].
75 As the GM of healthy adult subjects is typically < 5 mm thick, spatial smoothing needs to be carefully
76 performed to retain the sensitivity and specificity of the underlying changes [26, 27]. Surface-based

77 approaches have been proposed with improved sensitivity in cortical morphometry [25, 28-33] over
78 volumetric neuroimaging in both fMRI and cortical features of interest. There is wide agreement that
79 the surface-based morphometric (SBM) analyses [34-36] have theoretical and empirical advantages
80 over traditional voxel-based morphometry (VBM) approaches for addressing the problem of inference
81 in group studies. However, substantial inter-subject variation in the shapes of local features (e.g., mean
82 curvature) still hampers accurate cortical surface registration.

83
84 A majority of studies focus on volume- or surface-based analysis on a particular modality [11, 37, 38].
85 Few studies [32, 38-40] have incorporated multi-modalities into a single integrated pipeline of surface-
86 based analyses. The desire to better understand structural-functional relationships drives the need for
87 robust analysis frameworks. The Human Connectome Project (HCP) minimal preprocessing pipeline
88 [38] is one such approach that integrates multimodal data for cross subject analysis. It is built upon the
89 FreeSurfer software tool (<https://surfer.nmr.mgh.harvard.edu>) for surface generation and alignment to
90 standard space in addition to defining Connectivity Informatics Technology Initiative (CIFTI) format
91 and grayordinate system that incorporates cortical and subcortical information. In a recent study,
92 multimodal surface matching (MSM) [41] registration is incorporated into a pipeline that uses
93 multimodal registration features containing myelin maps (Glasser and Van Essen, 2011), resting-state
94 networks (RSNs) and visuotopic features to drive alignment to a group template. In the HCP approach
95 [38], the data acquisition protocol is customized and often requires newly developed preprocessing
96 methods unlike conventional data acquisition schemes.

97
98 There is huge amount of clinical data that is already acquired from healthy individuals and also in
99 different clinical populations that is not acquired as per the HCP proposed standards. Having tools that
100 could provide HCP-style analyses to leverage the existing data to the extent possible will be beneficial
101 for clinical research. The ciftify pipeline [42] bridges the gap for making HCP-style analysis
102 applicable to non-HCP (i.e., legacy) datasets by adapting the key modules from HCP pipeline into
103 existing structural workflows. For functional/diffusion MRI data, the alignment with anatomical T1
104 plays an important role to map volume data onto the surface. Thus, preprocessing choices need to be
105 made to maximize the data quality given its limitations in legacy datasets. The ciftify pipeline takes the
106 preprocessed data from other modalities and converts it into needed grayordinate format for further
107 analysis.

108
109 In this paper, we propose N-GSBSS for carrying out localized statistical testing of neuroimaging data
110 across multiple modalities in GM. Unlike the skeletonization approach in GBSS, cortical surfaces
111 reconstructed from high resolution T1 images are employed to facilitate cross-subject analysis. This
112 method provides a bridge between volume and surface registration approaches to achieve cross-subject
113 correspondence of low resolution image data. This method is an extension of our previous work, GS-
114 BSS [24]. While conceptually similar, improvements are made in registration methodology that allow
115 mapping of the metrics of interest in subject space. The key idea in this method is to incorporate
116 normal search from the cortical surface to get metrics from highly probable GM voxels using the
117 orientation dispersion index (ODI) from the NODDI model. ODI is higher in GM compared to that of
118 WM [43], thus searching for higher ODI could help to locate underlying highly probable GM. Toward
119 this end, we show an application to statistical analysis of fMRI data. To test the sensitivity of the
120 approach, a simulation study is performed by varying region of interest (ROI) size and percentage
121 change of intensity values within the ROI. It is presented as a full end-to-end pipeline to perform such
122 spatial statistics in group analysis. We evaluated the performance of N-GSBSS against three baseline
123 pipelines: volume-based registration (VBR), FreeSurfer's surface registration (SBR) and ciftify
124 pipeline for fMRI and simulation studies. The source code for N-GSBSS is made available at
125 <https://github.com/MASILab/N-GSBSS/>. The computational time of N-GSBSS is 68 times faster than
126 that of traditional SBR or 86 times faster than the ciftify pipeline method [42].

127

128 **2. Methods**

129 **2.1. Background**

130 GS-BSS method was proposed to perform voxel-based statistical analysis of diffusion microstructure
131 features acquired at low resolution on GM surfaces using high-resolution T1 images. Structural images
132 are segmented and normalized to MNI template space using diffeomorphic anatomical registration using
133 exponentiated lie algebra (DARTEL) method [44]. Diffusion metrics of interest are co-registered to
134 structural T1 and transformed to MNI template space using forward deformation. GM surfaces are
135 deformed to MNI template space using inverse transformation obtained from the registration step.
136 Correspondence between cortical surfaces is obtained with diffeomorphic spectral matching DSM [45]
137 and the mapping is applied to the deformed diffusion microstructure data in MNI template space to
138 project onto the target surface for group analysis. GS-BSS is shown to yield better performance compared
139 to that of VBM or the skeletonization approach of GBSS, which is based on alignment invariant skeleton
140 projection. However, there are some methodological limitations that could impact the sensitivity of such
141 analysis. First, the possibility of having any misalignment between diffusion microstructure and structural
142 images after co-registration, could impact the sensitivity of the analysis to be performed on highly
143 probable GM region. Second, the diffusion metrics of interest are projected onto the GM cortical surface
144 in MNI template space that could allow the prospect of including distortions caused in the data from the
145 volume registration step. Finally while the GM surfaces are used for achieving cortical correspondence,
146 all the data is mapped back into voxel-space before performing statistical analysis.

147 In this paper, the goal is to improve spatial statistics in GM by projecting all the metrics of interest from
148 each modality onto a single target cortical surface and carry out vertex based statistical analysis. Current
149 work addressed the limitations of GS-BSS and provided improvement in the following areas,

- 150 • To overcome possible alignment issues from co-registration step and improve intra-subject
151 correspondence, cortical search is proposed that can further improve the sensitivity of the method.
- 152 • To minimize distortions and keep the data as close to the raw images that are acquired as
153 possible, metrics of interest are mapped onto the cortical surface in subject space unlike the GS-
154 BSS method where the metrics of interest are mapped from the volume image in MNI space onto
155 the deformed cortical surface in MNI template space.
- 156 • To perform spatial statistics on vertices, unlike the voxel based spatial statistics that is performed
157 in GS-BSS.
- 158 • To show applicability of the method in additional modalities like fMRI.

159 **2.2. Subjects and neuroimaging data acquisition**

160 Neuroimaging data were collected on 30 healthy subjects (average age = 31.94 (male, n=18) / 35.83
161 (female, n=12)) who participated in an on-going study of brain connectivity in neuropsychiatric disorders.
162 The Vanderbilt University Institutional Review Board approved the study and all participants provided
163 written informed consent prior to enrolling in the study. Neuroimaging data were acquired on a 3T
164 scanner (Achieva, Philips Medical Systems, Best, The Netherlands) equipped with a 32-channel head coil
165 located at the Vanderbilt University Institute of Imaging Sciences. The following neuroimaging data were
166 acquired on each subject: 1) a T1-weighted 3D-TFE anatomical scan (1 mm isotropic resolution,
167 TE=2ms, TR=8.95 ms and TI=643 ms), 2) up to 6 functional EPI scans (3 mm resolution during which
168 subjects completed an event related spatial working memory task (described below), and 3) a diffusion-

169 weighted imaging scan protocol (2.5 mm isotropic resolution, with a matrix of 96 x 96, 50 slices,
170 TR=2.65s, TE=101ms, Gmax = 37.5 mT/m) that included two diffusion shells with b-values of 1000
171 s/mm² (24 directions) and 2000 s/mm² (60 directions). Two subjects are excluded from the diffusion
172 processing due to motion-related quality issues in diffusion MRI acquisition. HARDI from one subject is
173 marked unusable due to zipper artifact in B0. Second subject is excluded based on quality checking
174 measures due to subject movement (15 mm movement). Cardiac and respiratory gating were not used.

175 **2.3. Preprocessing**

176 **2.3.1. T1 anatomical data processing**

177 Each structural scan was segmented into GM, WM, and cerebrospinal fluid (CSF) tissue classes using the
178 VBM8 toolbox (<http://dbm.neuro.uni-jena.de/vbm/>) from SPM12 (<http://www.fil.ion.ucl.ac.uk/spm>).
179 Additionally, each voxel of the images was automatically labeled using multi-atlas segmentation [46]
180 according to the BrainCOLOR protocol [47] into 132 brain regions and 1 background that was used as a
181 preprocessing step for MaCRUISE . The white, central and pial cortical surfaces were reconstructed by
182 MaCRUISE [48] using the topology-preserving geometric deformable surface model. The central surfaces
183 were used in further surface-based processing including registration and mapping volume data onto the
184 surfaces.

185 **2.3.2. Diffusion data processing**

186 Diffusion-weighted images (DWI) were preprocessed using EDDY [49] tool from FMRIB Software
187 Library FSL [50] for eddy current correction and subject motion correction. The registration matrix of
188 each DWI was used to measure patient movement, and the gradient table was rotated accordingly. For
189 diffusion data processing, the data from 2 shells were combined into a single DWI file and corresponding
190 b-values and b-vectors were concatenated accordingly. A scheme file was generated using the fsl2scheme
191 command from Camino (<http://camino.cs.ucl.ac.uk>). A brain mask was created using the FSL brain
192 extraction tool.[51]

193 For NODDI processing, the DWI file, scheme file and mask (generated as described above) were passed
194 to the AMICO package (<https://github.com/daducci/AMICO/>), which is a fast implementation of NODDI
195 [43] with linear approximation. Single transformation was derived using b0 image to co-register to
196 structural T1-weighted scan using spatial normalization from SPM12 with 12-parameter affine
197 registration. Corresponding transformation is applied to NOODI-derived maps of intracellular volume
198 fraction, isotropic volume fraction (V_{iso}), and orientation dispersion index (ODI). These ODI and V_{iso}
199 maps from multiple subjects were used in further analysis and validation of N-GSBSS.

200 **2.3.3. Working memory fMRI processing**

201 During the functional EPI scans, subjects completed a slow event-related spatial working memory task.
202 Briefly, on each trial, three filled circles were presented sequentially, one at a time, during a 3-second
203 encoding phase. The encoding phase was followed by a 16 second delay period during which a fixation
204 dot was shown. Following the delay period, a probe (open circle) was presented for 1 second and subjects
205 had to indicate with a button press whether or not the probe matched one of the previously encoded
206 locations. Each trial was followed by a 14 second inter-trial interval. Subjects complete 30 working
207 memory trials and 18 control trials. The working memory and control trials were identical, except for the
208 fact that subjects were asked not to memorize the locations during the cue period of the control trials and
209 pressed both the yes and no button during the probe period. Different colored circles, red and grey, were
210 used to alert subjects to working memory and control trials, respectively. Preprocessing and generation of
211 first-level, subject-specific statistical parametric maps were performed using spatial normalization in

212 SPM12 [52]. Preprocessing included slice timing and motion correction, and co-registration of each
213 subject’s functional EPI scans to their anatomical T1-weighted scans. Subject-specific, voxel-wise maps
214 showing relative difference in the BOLD response between working memory and un-modeled baseline
215 for cue, maintenance, and probe conditions were generated by modeling each subject’s time series data.
216 Note, the contrast maps for cue, maintenance, and probe conditions were kept in the individual subject-
217 specific space co-registered to T1 prior to being entered into the N-GSBSS pipeline described below.

218 **2.4. N-GSBSS pipeline**

219 The steps involved in carrying out the spatial statistics starting from the preprocessed multi-modal data to
220 transferring all the metrics of interest onto a single target surface are illustrated in this section. The data
221 from the co-registered volume images is projected onto the GM central surface using enclosing voxel
222 approach. Alignment issues after co-registration would introduce partial volume effects or outliers by
223 fetching data from the voxels that may not belong to highly probable GM. In order to overcome this
224 limitation, cortical search is implemented using ODI measure as it has been shown to be higher in GM
225 compared to that of WM [43].

226 **2.4.1. Cortical search using NODDI maps**

227 Diffusion microstructure indices from NODDI including ODI and V_{iso} are used in the cortical search.
228 First ODI is masked with V_{iso} to exclude any voxels with isotropic volume fraction of greater than 0.5
229 indicating CSF regions. The surface normal is calculated at each vertex on the central surface. As the T1
230 was acquired at 1 mm resolution and the cortical thickness is < 5 mm thick, we search the maximum ODI
231 at each vertex along positive and negative normal directions (2 mm at maximum range with an interval of
232 1 mm). We create a search map by collecting these enclosing voxels that the normal directions point out.
233 The metrics of interest in other modalities are finally transferred onto the central surface via the search
234 map. Fig 2(a) illustrates this approach and corresponding histogram of masked ODI is shown in Fig 2(b)
235 before and after search.

Fig 2: (a) ODI overlaid with cortical surface mapping based on enclosing voxels, 1 mm above, 2 mm above, 1 mm below and 2 mm below of central surface obtained using normal search. At each vertex, maximum ODI value is selected from these 5 values along the vertex normal (white arrow in zoomed in box) and corresponding map is used for projecting the diffusion metrics on to the cortical surface. (b) Histogram of ODI projected on to the cortical surface on single subject before and after ODI search.

236

237 **2.4.2. Cortical correspondence on the target surface**

238 Cortical surfaces are highly variable, so roughly similar surfaces would be useful for surface registration.
239 As preprocessing volume registration can provide reasonably well-aligned surfaces, structural T1 is non-
240 linearly registered with MNI template using ANTs SyN registration method (52). Corresponding inverse
241 deformation is applied to the surface as the first step. The vertex coordinates of the surface are converted
242 to RAS format before applying “antsApplyTransformsToPoints” from ANTs toolbox. The deformed
243 coordinates are converted back into original format thus transforming the surface from subject space to
244 MNI space (#2 from Figure 3). However, as shown in Figure 1(a), the cortical anatomy is not yet well
245 aligned across the subjects after volume deformation. Then, we refine/update the correspondence using
246 surface registration step [45] in the same way as (24), which is expected to establish better
247 correspondence. It provides mapping information of the cortical surface from each subject onto the target
248 surface (#3 from Figure 3) on which spatial statistics can be performed.

Fig 3: Flowchart of the N-GSBSS data processing for each subject. (1) The central surface is reconstructed via MaCRUISE (red) (2) and transformed to the MNI space (yellow) using ANTs volume registration. (3) These volumes are diffeomorphically registered to a single target surface. (4) Metrics of interest in other modalities are co-registered to corresponding anatomical T1-weighted image. (5) Cortical ODI search is performed using ODI and V_{iso} from NODDI metrics to search for higher ODI excluding V_{iso} within a given range (6) Data are processed for each modality (NODDI for diffusion microstructure and first level analysis for working memory tasks) to derive metrics of interest for cross-sectional analysis. (7) Metrics of interest are mapped onto the individual surface. (8) The mappings from shape correspondence are used to project intensity values of metrics of interest to the target surface (blue). (9) Vertex-wise spatial statistics on all projected data are performed on the target surface.

249

2.4.3. Project metrics of interest on target surface

250 As cortical anatomical properties such as cortical thickness were derived from the surface, they were
251 already assigned to each vertex. These properties were then projected onto the target surface via the
252 established shape correspondence from step 3. Images from different modalities are co-registered to T1
253 anatomical images before proceeding with further analysis as shown in step 4. Cortical ODI search is
254 performed by taking in ODI and V_{iso} measures from the NODDI model to get the corresponding map of
255 highly probable GM vertices for co-registered images (step 5 in Fig 3). Step 6 illustrates the first level
256 analysis carried out on each modality to derive metrics of interest. In the volume images, the metrics of
257 interest were mapped onto the individual GM surface (step 7 in Fig 3) from the voxel that encloses the
258 corresponding vertex coordinate obtained from the cortical ODI search (step 5 in Fig 3). Both dMRI
259 based NODDI metrics and fMRI based working memory contrast maps were projected via the vertex
260 coordinates and the mapped properties were then transferred onto a common target surface (Step 8 in Fig
261 3). Spatial statistics across the subjects are performed on the target surface by applying 2 mm smoothing
262 kernel for cross subject analysis. We adapted the Gaussian kernel smoothing proposed by [37, 38], where
263 each vertex was weighted based on data from the neighboring vertices and scaled by the vertex area.

264

2.4.4. Summary highlighting enhancements

265 A novel ODI search along surface normal for maximum ODI value is used to probe for highly probable
266 GM regions in the co-registered image. Additionally, enhancements that are made to the earlier method
267 [24] are the transfer of metrics of interest on to the GM cortical surface in the individual subject space
268 instead of MNI space, to reduce the error that could occur with volume and surface deformation to the
269 MNI template. While [24] showed the application to diffusion microarchitecture features, this work
270 extends the applications to fMRI data, thus enabling multimodal analysis across structural and functional
271 changes. Group analysis is performed at vertex level on the target surface.

272 The evaluation of the approach is carried out in the following ways. 1) We compare qualitative mean
273 ODI, a diffusion microstructure feature, for N-GSBSS with and without cortical ODI based search in
274 comparison with ciftify pipeline. 2) We perform non-parametric permutation testing on contrast maps
275 obtained from first level analysis of working memory tasks in fMRI. 3) We perform a simulation study in
276 structural MRI to evaluate sensitivity and specificity of the approach.

277

2.5. Spatial statistics

278 Once all the properties from different modalities were projected on the target surface, GM based vertex-
279 wise spatial statistics were calculated using the Permutation Analysis of Linear Models (PALM) [53]
280 package from the FSL software library (FMRIB; <http://www.fmrib.ox.ac.uk/fsl/>) which performs
281 inference through permutation. Significant results are reported after controlling for family-wise error
282 (FWE) with $p < 0.05$ through threshold free cluster enhancement (TFCE).

283
284
285
286
287
288
289
290
291
292

293

294
295
296
297
298
299
300

301

302
303
304
305
306
307
308
309
310
311
312
313
314
315
316
317
318

319
320
321

322

323

324

2.6. Baseline methods

2.6.1. Volume based registration (VBR) processing

Volume images of metrics of interest from other modalities were registered to MNI template by applying the non-rigid transformation obtained from anatomical T1-weighted images. A GM mask was calculated based on 0.5 thresholds on the GM probability map in each subject and 70 percent overlap across all the subjects to filter the number of voxels to retain highly probable GM voxels. Gaussian kernel smoothing of 2 mm was applied before performing spatial statistics. Nonparametric permutation based testing was performed on smoothed volume data within a brain mask using FSL PALM [53] (<https://fsl.fmrib.ox.ac.uk/fsl/fslwiki/PALM>). Statistical results were projected onto the target surface based on the enclosing voxel approach for visualization and comparison with surface based results.

2.6.2. Surface based registration (SBR) processing

In order to compare the proposed approach, we used the FreeSurfer surface registration method [30] for cortical shape correspondence. Metrics of interest from volume data in subject space were projected onto the central surface using the enclosing voxel approach. These metrics were transferred to the target surface via the shape correspondence and smoothed on the target surface for cross-sectional analysis. In order to make a fair comparison with N-GSBSS results with optimal multiple comparison correction, metrics of interest from two hemispheres were considered as a single dataset before carrying out the permutation based statistical tests.

2.6.3. Ciftify pipeline processing

The ciftify pipeline [42] has been developed to facilitate grayordinate-based analysis in CIFTI format for legacy datasets. In preprocessing, surface reconstruction is carried out using `ciftify_recon_all` command that takes `recon_all` FreeSurfer 6.0 (<https://surfer.nmr.mgh.harvard.edu>) outputs and generate CIFTI file for structural measures (e.g., cortical thickness) from the surface. The distortion corrected dMRI images are registered to their own structural T1 images by FMRIB Software Library's (FSL 5.0) FLIRT [54]. First rigid alignment is performed followed by the boundary-based registration by supplying WM segmentation obtained from FreeSurfer as an input argument. For fMRI processing, preprocessed first level images are co-registered to their own structural T1 image using SPM12. Conversion tools provided in ciftify toolbox are used to put preprocessed dMRI data and fMRI data into grayordinates in CIFTI format for further analysis. To project diffusion measures from volume onto the cortical surfaces, a ribbon mapping method is used, in which the volumetric measures are collected along the GM ribbon defined by white and pial surfaces, as described in [16]. Unfortunately, there are no T2 weighted images available in our custom dataset. Thus, myelin-style volume to surface mapping is infeasible for our diffusion analysis since myelin maps are unavailable. The grayordinates are based on the low-resolution standard mesh (with ~32k vertices in each hemisphere) at 2 mm resolution with a total of ~64k cortical vertices for both hemispheres obtained with the default settings. The low-resolution standard mesh is the suggested template that is appropriate for cross-subject analysis of low-resolution data like dMRI or fMRI.

Processing time comparison between N-GSBSS and SBR using FreeSurfer are reported in Table 1. We used a single thread (Intel Xeon CPU E5-2630 v4 @ 2.20GHz and 32 GB of RAM) on an Ubuntu 16.04 LTS Linux Workstation.

Pipeline	Processing steps details	Total time
SBR	Per hemisphere: FSRUNTIME@ mris_sphere 1.48 hours, 1 thread FSRUNTIME@ mris_register 0.80 hours, 1 thread	~273.6 mins
Ciftify	ReconAll (mris_sphere and mris_register) : 4.71 hours hrs, 1 thread Ciftify : 1hr 5 mins, 1 thread	~345 mins
N-GSBSS	ANTs volume registration: ~2.12 mins, 1 thread DSM surface registration: ~1.49 mins, 1 thread	~4 mins

325 **Table 1** Processing time comparison for SBR, ciftify and N-GSBSS based approaches. In SBR, a
326 spherical mapping was conducted for each hemisphere followed by spherical registration. Details of
327 time taken for each step are provided in the processing details column.
328

329 2.7. Simulation study setup

330 The spherical masks with a radius of 3, 4, and 5 mm were created in template space and transferred back
331 to subject space via the inverse transformation from ANTs SyN [55] registration for each subject. This
332 range was chosen since the cortex is around <5 mm thick and because capturing the ROIs with different
333 radii could reflect the differences in accounting for partial volume effects in the GM and WM border
334 regions. The location was chosen to contain cortical folding that is variable across multiple subjects to
335 account for partial volume effects when performing cross subject studies.

336 The GM probability maps for the 30 subjects were randomly divided into two groups, G1 and G2, with 15
337 subjects in each group. The GM probability data in G2 were then modified in the subject space to
338 simulate percentage change of intensity values in intervals of 10% in the corresponding mask regions. A
339 total of 27 combinations (3 masks and 9 different scalings) were considered for evaluation.

340 With 0% change, the images in G2 were the same as original images. Thus, we considered the difference
341 between the groups as a baseline. We excluded 100% change of the region of interest in G2, which is
342 completely reduced to zero. With 50% change, the intensity values were half of the original values in
343 ROIs from G2 images.

344 GM probability data from each of the 27 combinations in G2 were then processed through N-GSBSS to
345 place all the data on the target surface for cross-sectional analysis. GM probability data were also
346 evaluated for VBR, SBR and ciftify for comparison with the same parameter/experimental settings,
347 including 2 mm Gaussian kernel smoothing. Non-parametric permutation tests were then performed
348 between G1 and G2 for all combinations using FSL’s PALM [53] package with 5000 iterations.

349 To assess the sensitivity of the approaches, we examined the ratio of maximum t-statistic (“t-stat ratio”),
350 which was defined as the amount of scaling with respect to the baseline. To have a single metric with
351 comparable result across all the methods, we reported the ratio with respect to baseline. Baseline is where
352 we performed second level analysis for group differences across the 2 groups where no changes are
353 applied to original GM probability maps.

354 3. Results

355 In this section, we present the results of all the N-GSBSS analysis as follows: 1) Qualitative results of
356 mean ODI with and without search in comparison with the ciftify pipeline 2) Application in fMRI to

357 identify active regions in task based working memory. 3) GM simulation results in structural MRI based
358 on varying ROI size and intensity differences.

359 Mean ODI values across 30 subjects are shown on the target surface (Fig 4) for N-GSBSS without search,
360 with cortical ODI search and the ciftify pipeline. With cortical ODI search, partial volume effects are
361 addressed reflecting higher ODI across the cortex compared to that of other two approaches.

Fig 4: Mean ODI across 28 healthy subjects using (a) N-GSBSS – S0 with no search (a) N-GSBSS - S2 including ODI search of 2 mm (c) ciftify pipeline. The ciftify results are based on the “gray ordinates” with 64 thousand vertices (the suggested tessellation) on both left and right hemispheres while the target surface template used in N-GSBSS has about 261 thousand vertices.

362

363 **3.1. Working memory fMRI results**

364 As an application of N-GSBSS in fMRI, working memory data was processed for 30 healthy subjects
365 in cue, probe and delay tasks. We compared significant regions revealed by VBR, SBR, the ciftify
366 pipeline and N-GSBSS methods as shown in Fig 5. For all these tasks, the overall activation pattern is
367 comparable across different methods. As expected, the significant vertices in VBR are fewer and more
368 scattered than the cortical surface-based approaches of SBR, ciftify and N-GSBSS.

Fig 5: Working memory fMRI data were processed for 28 healthy controls and results are reported for (a) correct cue, (b) correct delay (c) correct probe tasks with 2 mm smoothing for VBR, SBR, ciftify, N-GSBSS -S0 with no search and N-GSBSS-S2 with 2mm search methods. Significant p-values after FWE correction based on non parametric randomize one sample t-test with 10000 iterations are reported. $P_{fwe} < 0.05$ are highlighted in red.

369

370 Quantitative representation of the number of significant vertices with $p < 0.05$ for all the three tasks are
371 shown in Fig 6. Note that N-GSBSS has a higher number of significant vertices in all the tasks than
372 VBR, SBR and ciftify pipeline results. The ciftify pipeline results are comparable to that of N-GSBSS
373 more than VBR or SBR approaches. Applying cortical ODI search further improved the activation
374 percentage in N-GSBSS.

Fig 6: Percentage activation of working memory fMRI data were processed for 28 healthy controls and results are reported for (a) correct cue, (b) correct delay (c) correct probe tasks with 2 mm smoothing for VBR, SBR, ciftify, N-GSBSS –S0 with no search and N-GSBSS –S2 with 2mm search methods. The number of significant vertices, with p-values < 0.05 after FWE correction based on nonparametric randomize one sample t-test with 10000 iterations, is divided by total number of vertices and the percentage is reported.

375

3.2. Simulation study in structural MRI with changes in regions of interest

Here, we evaluate N-GSBSS with respect to VBR, SBR and ciftify pipeline techniques in identifying sensitivity and specificity of changes in GM voxels located in spherical ROIs of 3, 4, and 5 mm radius located in a region of the frontal cortex. Fig 7 illustrates spheres with a radius of 5 and 3 mm.

Fig 7: The gray matter probability map shows the simulated effect as an overlay mask of 5 mm (red) and 3 mm (dark blue) spheres.

Quantitative results in Fig 8 show the t-statistics ratio for varying ROI sizes of 3 mm, 4 mm, and 5 mm, and percentage change in the GM probability values from 10% to 90% in the intervals of 10%. T-stat ratio is the maximum t-statistic for each scenario with respect to the baseline to reflect how much it was scaled with induced changes in the region of interest. The baseline is chosen to be the differences between the 2 groups in the current experiment. For VBR, to capture the intensity difference between groups, the probability change must be at least 40% with 5 mm spherical ROI, 50% for 4 mm, and 60% for 3 mm ROI. SBR results showed sensitivity for 20% change with 5 mm ROI. However little difference is observed between baseline and 4 mm ROI from 40% and no difference was captured with 3 mm ROI. N-

Fig 8: Quantitative results for statistical group differences over the change in ROI size from 3 to 5 mm and percentage change from 10 percent to 90 percent. (a) Results from VBR analysis. (b) Results from FreeSurfer registration analysis. (c) Results from ciftify pipeline with default gray ordinates. (d) Results from GSBSS based analysis. Y-axis indicates maximum t-statistic ratio with respect to baseline. X-axis indicates the percentage change of GM probability in G2 with respect to original GM probability images in G2.

GSBSS results are much more sensitive starting at 10% with 5 mm ROI, 20% with 4 mm and 30% for 3 mm spherical ROI. N-GSBSS also showed higher maximum t-statistics than SBR. With higher intensity differences starting at 70%, VBR results have higher t-statistic ratio than that of N-GSBSS. In all other cases N-GSBSS has higher maximum t-statistic ratio and better sensitivity.

4. Discussion

Herein, we describe an approach for carrying out multi-modal spatial statistics in low resolution images by taking advantage of high resolution T1 weighted images that are acquired as part of the scan protocol. This approach favorably compares with traditional volume based analyses and with respect to the FreeSurfer surface registration approach along with the ciftify pipeline. Our approach offers an advantage over VBM by achieving improved cortical alignment in agreement with other surface-based registration techniques [25, 28-33]. Moreover, in comparison with FreeSurfer, SBR, and ciftify pipelines, the N-GSBSS approach showed an improvement in sensitivity. It suggests that the initial alignment obtained by non-rigid deformation from the T1 image provides a deformed cortical shape that makes surface registration much easier. Consequently, this improves the statistical power compared to existing approaches.

The key aspect of this work is the addition of NODDI based search, which ensures that metrics from low-resolution images are retrieved from highly probable GM. It is achieved by making use of the ODI

409 measure from NODDI which is known to be higher in GM compared to that of WM [43]. Thus by
410 searching for maximum ODI, alignment issues after co-registration or PVE effects from underlying
411 voxels is addressed. The patterns of mean ODI are comparable between these methods with higher
412 values along the gyral regions. The overall mean ODI values in ciftify approach appear to be less than
413 that of the GSBSS approach with or without search (Figure 4). Lower values could be due to the
414 partial volume effects arising from thinner cortex regions as acknowledged in Fukutomi et al.'s paper
415 [56] indicating the possibility of residual PVE effects in the regions of thinner cortex. When compared
416 to mean ODI values reported in Fukutomi et al.'s paper, the results indicated in our study have higher
417 ODI values across all the methods. Possible reason for this deviation could be due to the number of
418 differences between the two datasets like demographics, data acquisition, and processing. Also we
419 followed the original NODDI model which has empirical settings as mentioned below where $d_{||} =$
420 $1.7 \times 10^{-3} \text{ mm}^2/\text{s}$, to be representative of both white and gray matter on two-shell data ($b=1000/2000$
421 s/mm^2), while in Fukutomi et al., paper [56] $d_{||}$ is calculated to be $1.1 (0.1) \times 10^{-3} \text{ mm}^2/\text{s}$ for gray
422 matter from an empirically chosen range and the results reported are based on three-shell data
423 ($b=1000/2000/3000 \text{ s}/\text{mm}^2$). While the preliminary normal search proposed based on higher ODI
424 seems to improve sensitivity for the changes occurring in pure gray matter, these results may have to
425 be carefully reviewed if a regional variation is essential for the study of interest.

426 As we are interested in low resolution with dMRI acquired at 2.5 mm resolution and fMRI at 3 mm
427 resolution, we are assuming that after co-registration to T1, the underlying data is roughly aligned at
428 voxel level. Thus we utilize the search map obtained from diffusion modality to apply to fMRI for
429 getting the data based on enclosing voxel approach. The reported fMRI t-statistics suggest an
430 improvement in sensitivity with N-GSBSS. While there is no ground truth for validating the
431 implication of the higher activation, since the contrast maps are relative to that of the un-modeled
432 baseline across 30 subjects, the activation could indicate that the proposed method could be highly
433 sensitive to capture underlying variations that are indirectly contributing to the activations instead of
434 capturing the false positives.

435 The simulation study is set up to perform sensitivity or specificity check for N-GSBSS to the underlying
436 changes in tissue microstructure. As we are interested in performing analysis in psychiatric applications
437 including schizophrenia [57, 58] that are known to have changes in prefrontal region, the ROI is chosen
438 from this region. The GM probability map is chosen as the parameter of interest and the intensity changes
439 are simulated within an ROI region. Compared to the baseline methods, N-GSBSS showed superior
440 sensitivity to the underlying changes in both intensity and the size of the ROI as shown in Fig 8. While
441 volume-based analysis was not able to detect any significant differences between groups for at least up to
442 50% change in the GM probability values, N-GSBSS was able to capture differences starting from 10%
443 change with ROI size of 5 mm, 20% for 4 mm and 30% for 3 mm. The low performance of VBM could
444 be potentially due to partial volume effects prevalent in the volume-based approach even after applying
445 the GM mask to limit the analysis to highly probable GM regions.

446 In the simulation study, SBR analysis showed a similar pattern as N-GSBSS. However, the sensitivity of
447 this approach is not as high as N-GSBSS. Differences between the methods are likely due to different
448 registration approaches since both of them used the same surface to obtain corresponding GM probability
449 values from the volume image. The ciftify pipeline results are similar to those of SBR, which is expected
450 since the ciftify pipeline uses FreeSurfer registration. The subtle difference between ciftify and SBR are
451 observed likely due to the different surface reconstruction in each of these pipelines. For a fair
452 comparison, we used the ciftify pipeline with default parameters to the extent possible. For example, the
453 analysis results in the ciftify pipeline are based on the "gray ordinates" with 64k vertices (the suggested
454 tessellation for cross subject analysis of low resolution data) on both left and right hemispheres. This
455 surface tessellation differs from that of the target central surface used in SBR and N-GSBSS analysis
456 (about 261k vertices for both hemispheres). This could have contributed to the lower sensitivity of ciftify

457 pipeline in this simulation study due to the limited ability to capture smaller ROI regions with less
458 number of vertices. The higher sensitivity of N-GSBSS to capture GM probability percentage changes as
459 low as 10% for 5 mm ROI and 40% for smaller ROI of 3 mm ROI could indicate that it is able to capture
460 more number of highly probable vertices accurately. In future, additional validations could be performed
461 to evaluate the performance for different resolutions and also at different ROI locations.

462 **5. Conclusion**

463 Overall significant regions captured by N-GSBSS agree with those of VBR, SBR, and ciftify pipelines
464 across different modalities while achieving high spatial specificity. It is highly likely that the volumetric
465 transformation already deformed cortical surfaces into similar shapes (geometry) before the surface
466 registration, which results in better shape correspondence by reducing the local anatomical ambiguity in
467 the surface registration. N-GSBSS possesses high flexibility that allows any registration method as well
468 as multiple modalities. We expect that such a feature can be generally extended to various modalities in
469 general neuroimaging studies.

470 An operational virtual machine and source code for N-GSBSS are posted in a Docker image:
471 (<https://github.com/MASILab/N-GSBSS/>).

472

473 **6. Acknowledgements**

474 This work was conducted in part using the resources of the Advanced Computing Center for Research and
475 Education at Vanderbilt University, Nashville, TN. This project was supported in part by the National
476 Center for Research Resources, Grant UL1 RR024975-01, and is now at the National Center for
477 Advancing Translational Sciences, Grant 2 UL1 TR000445-06 and NIH R01EB017230 &
478 R01MH102266. The content is solely the responsibility of the authors and does not necessarily represent
479 the official views of the NIH.

480

481 **7. References**

- 482 1. Woodward ND. Thalamocortical Functional Connectivity, Cognitive Impairment, and Cognitive
483 Remediation in Schizophrenia. *Biological Psychiatry: Cognitive Neuroscience and Neuroimaging*. 2017;2(4):307-9.
- 484 2. Gennatas ED, Avants BB, Wolf DH, Satterthwaite TD, Ruparel K, Ciric R, et al. Age-related effects and
485 sex differences in gray matter density, volume, mass, and cortical thickness from childhood to young adulthood.
486 *Journal of Neuroscience*. 2017;37(20):5065-73.
- 487 3. Gold AL, Steuber ER, White LK, Pacheco J, Sachs JF, Pagliaccio D, et al. Cortical Thickness and
488 Subcortical Gray Matter Volume in Pediatric Anxiety Disorders. *Neuropsychopharmacology*. 2017.
- 489 4. Gong NJ, Chan CC, Leung LM, Wong CS, Dobb R, Liu C. Differential microstructural and morphological
490 abnormalities in mild cognitive impairment and Alzheimer's disease: Evidence from cortical and deep gray matter.
491 *Human Brain Mapping*. 2017;38(5):2495-508.
- 492 5. Korponay C, Dentico D, Kral T, Ly MM, Kruis A, Goldman R, et al. Neurobiological correlates of
493 impulsivity in healthy adults: lower prefrontal gray matter volume and spontaneous eye-blink rate but greater
494 resting-state functional connectivity in basal ganglia-thalamo-cortical circuitry. *NeuroImage*. 2017.
- 495 6. Tóth E, Szabó N, Csete G, Király A, Faragó P, Spisák T, et al. Gray Matter Atrophy Is Primarily Related to
496 Demyelination of Lesions in Multiple Sclerosis: A Diffusion Tensor Imaging MRI Study. *Frontiers in*
497 *neuroanatomy*. 2017;11.
- 498 7. Calhoun VD, Adali T, Giuliani NR, Pekar JJ, Kiehl KA, Pearlson GD. Method for multimodal analysis of
499 independent source differences in schizophrenia: combining gray matter structural and auditory oddball functional
500 data. *Hum Brain Mapp*. 2006;27(1):47-62.

501 8. Shen D, Cui L, Fang J, Cui B, Li D, Tai H. Voxel-Wise Meta-Analysis of Gray Matter Changes in
502 Amyotrophic Lateral Sclerosis. *Front Aging Neurosci.* 2016;8:64.

503 9. Nazeri A, Mulsant BH, Rajji TK, Levesque ML, Pipitone J, Stefanik L, et al. Gray Matter Neuritic
504 Microstructure Deficits in Schizophrenia and Bipolar Disorder. *Biol Psychiatry.* 2017;82(10):726-36.

505 10. Ekman CJ, Petrovic P, Johansson AG, Sellgren C, Ingvar M, Landén M. A History of Psychosis in Bipolar
506 Disorder is Associated With Gray Matter Volume Reduction. *Schizophrenia bulletin.* 2016;43(1):99-107.

507 11. Nazeri A, Chakravarty MM, Rotenberg DJ, Rajji TK, Rathi Y, Michailovich OV, et al. Functional
508 consequences of neurite orientation dispersion and density in humans across the adult lifespan. *J Neurosci.*
509 2015;35(4):1753-62.

510 12. Carmona S, Vilarroya O, Bielsa A, Tremols V, Soliva JC, Rovira M, et al. Global and regional gray matter
511 reductions in ADHD: a voxel-based morphometric study. *Neurosci Lett.* 2005;389(2):88-93.

512 13. Thompson PM, Hayashi KM, de Zubicaray G, Janke AL, Rose SE, Semple J, et al. Dynamics of gray
513 matter loss in Alzheimer's disease. *J Neurosci.* 2003;23(3):994-1005.

514 14. Von Economo C. *The cytoarchitectonics of the human cerebral cortex*: H. Milford Oxford University Press;
515 1929.

516 15. Von Economo C, Koskinas G. *The cytoarchitectonics of the adult human cortex*. Vienna and Berlin: Julius
517 Springer Verlag. 1925.

518 16. Glasser MF, Smith SM, Marcus DS, Andersson JL, Auerbach EJ, Behrens TE, et al. The Human
519 Connectome Project's neuroimaging approach. *Nat Neurosci.* 2016;19(9):1175-87.

520 17. Jones DK, Cercignani M. Twenty-five pitfalls in the analysis of diffusion MRI data. *NMR Biomed.*
521 2010;23(7):803-20.

522 18. Smith SM, Jenkinson M, Johansen-Berg H, Rueckert D, Nichols TE, Mackay CE, et al. Tract-based spatial
523 statistics: voxelwise analysis of multi-subject diffusion data. *Neuroimage.* 2006;31(4):1487-505.

524 19. Bodini B, Khaleeli Z, Cercignani M, Miller DH, Thompson AJ, Ciccarelli O. Exploring the relationship
525 between white matter and gray matter damage in early primary progressive multiple sclerosis: an in vivo study with
526 TBSS and VBM. *Human brain mapping.* 2009;30(9):2852-61.

527 20. Westlye LT, Walhovd KB, Dale AM, Bjørnerud A, Due-Tønnessen P, Engvig A, et al. Life-span changes
528 of the human brain white matter: diffusion tensor imaging (DTI) and volumetry. *Cerebral cortex.* 2009;20(9):2055-
529 68.

530 21. Olson EA, Cui J, Fukunaga R, Nickerson LD, Rauch SL, Rosso IM. Disruption of white matter structural
531 integrity and connectivity in posttraumatic stress disorder: A TBSS and tractography study. *Depression and anxiety.*
532 2017;34(5):437-45.

533 22. Bells S, Lefebvre J, Prescott SA, Dockstader C, Bouffet E, Skocic J, et al. Changes in white matter
534 microstructure impact cognition by disrupting the ability of neural assemblies to synchronize. *Journal of*
535 *Neuroscience.* 2017;37(34):8227-38.

536 23. Goodrich - Hunsaker NJ, Abildskov TJ, Black G, Bigler ED, Cohen DM, Mihalov LK, et al. Age - and
537 sex - related effects in children with mild traumatic brain injury on diffusion magnetic resonance imaging
538 properties: A comparison of voxelwise and tractography methods. *Journal of neuroscience research.*
539 2018;96(4):626-41.

540 24. Parvathaneni P, Rogers BP, Huo Y, Schilling KG, Hainline AE, Anderson AW, et al., editors. *Gray Matter*
541 *Surface based Spatial Statistics (GS-BSS) in Diffusion Microstructure*. International Conference on Medical Image
542 *Computing and Computer-Assisted Intervention*; 2017: Springer.

543 25. Jo HJ, Lee JM, Kim JH, Shin YW, Kim IY, Kwon JS, et al. Spatial accuracy of fMRI activation influenced
544 by volume- and surface-based spatial smoothing techniques. *Neuroimage.* 2007;34(2):550-64.

545 26. Bookstein FL. "Voxel-based morphometry" should not be used with imperfectly registered images.
546 *Neuroimage.* 2001;14(6):1454-62.

547 27. Crum WR, Griffin LD, Hill DL, Hawkes DJ. Zen and the art of medical image registration:
548 correspondence, homology, and quality. *Neuroimage.* 2003;20(3):1425-37.

549 28. Oosterhof NN, Wiestler T, Downing PE, Diedrichsen J. A comparison of volume-based and surface-based
550 multi-voxel pattern analysis. *Neuroimage.* 2011;56(2):593-600.

551 29. Dale AM, Fischl B, Sereno MI. Cortical surface-based analysis. I. Segmentation and surface reconstruction.
552 *Neuroimage.* 1999;9(2):179-94.

553 30. Fischl B, Sereno MI, Dale AM. Cortical surface-based analysis. II: Inflation, flattening, and a surface-based
554 coordinate system. *Neuroimage.* 1999;9(2):195-207.

555 31. Wandell BA, Chial S, Backus BT. Visualization and measurement of the cortical surface. *J Cogn Neurosci*.
556 2000;12(5):739-52.

557 32. Van Essen DC, Drury HA, Dickson J, Harwell J, Hanlon D, Anderson CH. An integrated software suite for
558 surface-based analyses of cerebral cortex. *J Am Med Inform Assoc*. 2001;8(5):443-59.

559 33. Yeo BT, Sabuncu MR, Vercauteren T, Ayache N, Fischl B, Golland P. Spherical demons: fast
560 diffeomorphic landmark-free surface registration. *IEEE transactions on medical imaging*. 2010;29(3):650-68.

561 34. Van Essen DC. A population-average, landmark-and surface-based (PALS) atlas of human cerebral cortex.
562 *Neuroimage*. 2005;28(3):635-62.

563 35. Fischl B, Sereno MI, Tootell RB, Dale AM. High-resolution intersubject averaging and a coordinate system
564 for the cortical surface. *Human brain mapping*. 1999;8(4):272-84.

565 36. Van Essen D, Drury H. Structural and functional analyses of human cerebral cortex using a surface-based
566 atlas. *Journal of Neuroscience*. 1997;17(18):7079-102.

567 37. Glasser MF, Sotiropoulos SN, Wilson JA, Coalson TS, Fischl B, Andersson JL, et al. The minimal
568 preprocessing pipelines for the Human Connectome Project. *Neuroimage*. 2013;80:105-24.

569 38. Glasser MF, Sotiropoulos SN, Wilson JA, Coalson TS, Fischl B, Andersson JL, et al. The minimal
570 preprocessing pipelines for the Human Connectome Project. *Neuroimage*. 2013;80:105-24.

571 39. Robinson EC, Jbabdi S, Glasser MF, Andersson J, Burgess GC, Harms MP, et al. MSM: a new flexible
572 framework for Multimodal Surface Matching. *Neuroimage*. 2014;100:414-26.

573 40. Glasser MF, Coalson TS, Robinson EC, Hacker CD, Harwell J, Yacoub E, et al. A multi-modal parcellation
574 of human cerebral cortex. *Nature*. 2016;536(7615):171-8.

575 41. Robinson EC, Garcia K, Glasser MF, Chen Z, Coalson TS, Makropoulos A, et al. Multimodal surface
576 matching with higher-order smoothness constraints. *NeuroImage*. 2018;167:453-65.

577 42. Dickie EW, Anticevic A, Smith DE, Coalson TS, Manogaran M, Calarco N, et al. ciftify: A framework for
578 surface-based analysis of legacy MR acquisitions. *bioRxiv*. 2018:484428.

579 43. Zhang H, Schneider T, Wheeler-Kingshott CA, Alexander DC. NODDI: practical in vivo neurite
580 orientation dispersion and density imaging of the human brain. *Neuroimage*. 2012;61(4):1000-16.

581 44. Ashburner J. A fast diffeomorphic image registration algorithm. *Neuroimage*. 2007;38(1):95-113.

582 45. Lombaert H, Sporring J, Siddiqi K. Diffeomorphic spectral matching of cortical surfaces. *Inf Process Med*
583 *Imaging*. 2013;23:376-89.

584 46. Asman AJ, Landman BA. Non-local statistical label fusion for multi-atlas segmentation. *Med Image Anal*.
585 2013;17(2):194-208.

586 47. Klein A, Dal Canton T, Ghosh SS, Landman B, Lee J, Worth A, editors. Open labels: online feedback for a
587 public resource of manually labeled brain images. 16th Annual Meeting for the Organization of Human Brain
588 Mapping; 2010.

589 48. Huo Y, Carass A, Resnick SM, Pham DL, Prince JL, Landman BA, editors. Combining multi-atlas
590 segmentation with brain surface estimation. *Proceedings of SPIE--the International Society for Optical Engineering*;
591 2016: NIH Public Access.

592 49. Andersson JLR, Sotiropoulos SN. An integrated approach to correction for off-resonance effects and
593 subject movement in diffusion MR imaging. *Neuroimage*. 2016;125:1063-78.

594 50. Smith SM, Jenkinson M, Woolrich MW, Beckmann CF, Behrens TE, Johansen-Berg H, et al. Advances in
595 functional and structural MR image analysis and implementation as FSL. *Neuroimage*. 2004;23 Suppl 1:S208-19.

596 51. Smith SM. Fast robust automated brain extraction. *Human brain mapping*. 2002;17(3):143-55.

597 52. Ashburner J, Friston KJ. Voxel-based morphometry--the methods. *Neuroimage*. 2000;11(6 Pt 1):805-21.

598 53. Winkler AM, Ridgway GR, Webster MA, Smith SM, Nichols TE. Permutation inference for the general
599 linear model. *Neuroimage*. 2014;92:381-97.

600 54. Jenkinson M, Bannister P, Brady M, Smith S. Improved optimization for the robust and accurate linear
601 registration and motion correction of brain images. *Neuroimage*. 2002;17(2):825-41.

602 55. Avants BB, Epstein CL, Grossman M, Gee JC. Symmetric diffeomorphic image registration with cross-
603 correlation: evaluating automated labeling of elderly and neurodegenerative brain. *Med Image Anal*. 2008;12(1):26-
604 41.

605 56. Fukutomi H, Glasser MF, Zhang H, Autio JA, Coalson TS, Okada T, et al. Neurite imaging reveals
606 microstructural variations in human cerebral cortical gray matter. *Neuroimage*. 2018;182:488-99.

607 57. Sheffield J, Parvatheni P, Rogers B, Landman B, Woodward N. T222. Functional Brain Activation and
608 Grey Matter Integrity in Psychosis: A Combined Functional Magnetic Resonance and Neurite Orientation
609 Distribution and Density Imaging Study. *Biological Psychiatry*. 2018;83(9):S214-S5.

610 58. Woodward ND, Parvatheni P, Rogers B, Damon S, Landman B, editors. Neurite orientation dispersion and
611 density imaging (NODDI) of the prefrontal cortex in psychosis. *Biological Psychiatry*; 2017: ELSEVIER SCIENCE
612 INC 360 PARK AVE SOUTH, NEW YORK, NY 10010-1710 USA.
613

614

615

616 **8. Supporting information**

- 617 • S1 File. Experiment data and processing guidelines.
- 618 • S2 File. Supplementary experimental validation results.

619

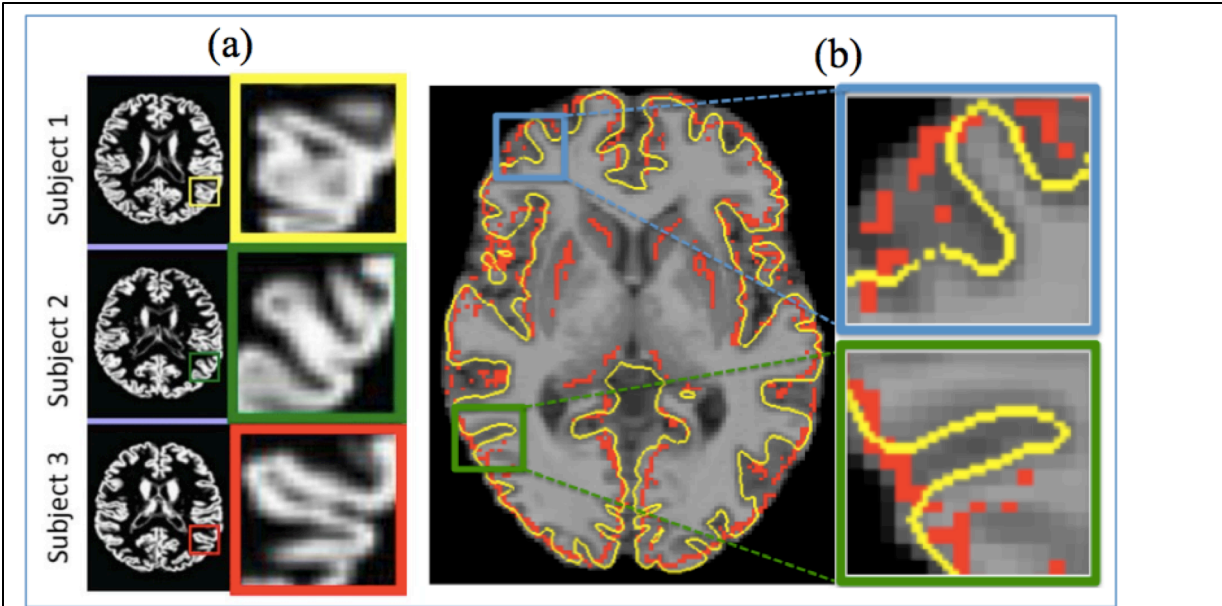


Fig 1: (a) Non-rigid image registration of GM probability maps of three subjects. Each color box highlights the corresponding region of interest. Right column shows detailed differences in cortical folding patterns across the subjects. (b) Skeletonized GM (red) and cortical central surface (yellow) are overlaid on T1 image. GM central surface closely follows the cortical structure compared to that of skeletonized GM approach. Two examples are highlighted in blue and green boxes where GM cortical surface closely follows the cortical structure compared to the volumetric based GM skeletonization approach. Darker regions on T1 indicate GM and lighter regions represent WM.

620

621

622

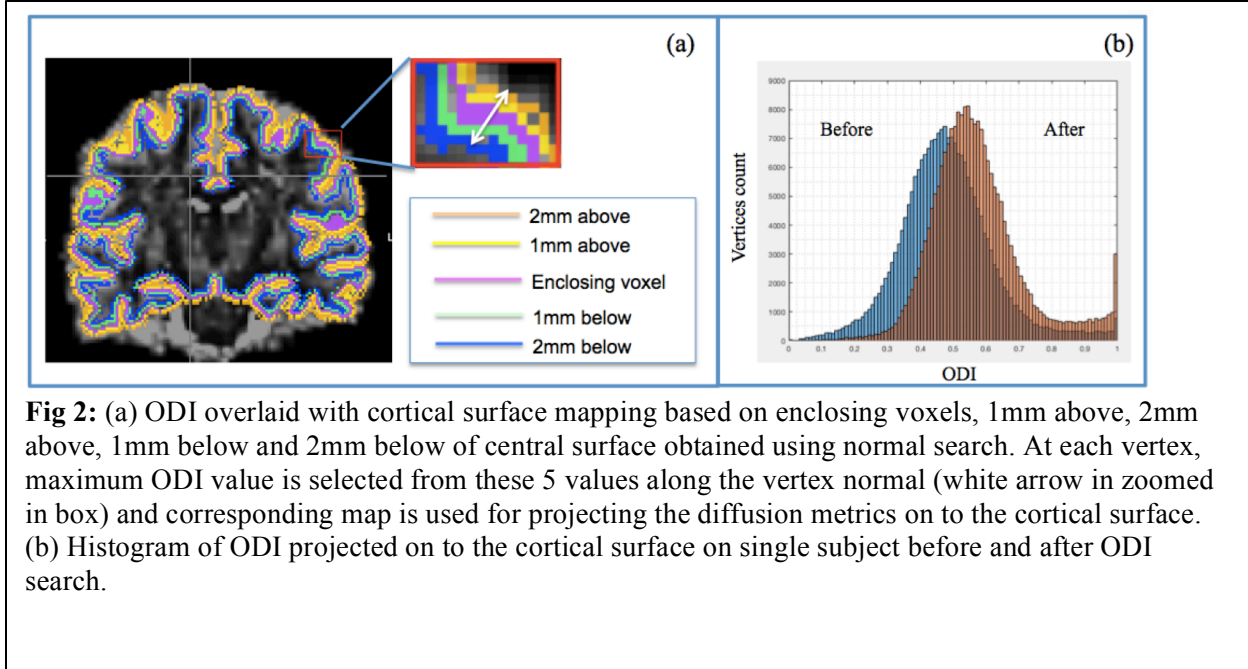


Fig 2: (a) ODI overlaid with cortical surface mapping based on enclosing voxels, 1mm above, 2mm above, 1mm below and 2mm below of central surface obtained using normal search. At each vertex, maximum ODI value is selected from these 5 values along the vertex normal (white arrow in zoomed in box) and corresponding map is used for projecting the diffusion metrics on to the cortical surface. (b) Histogram of ODI projected on to the cortical surface on single subject before and after ODI search.

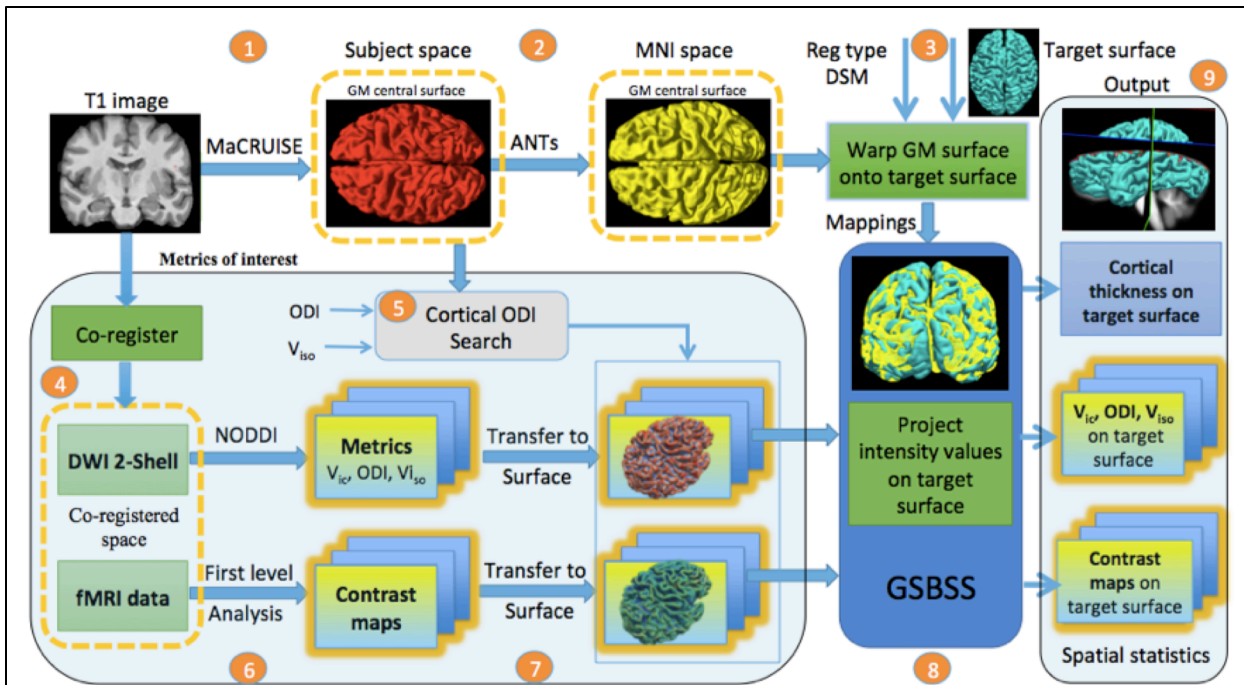
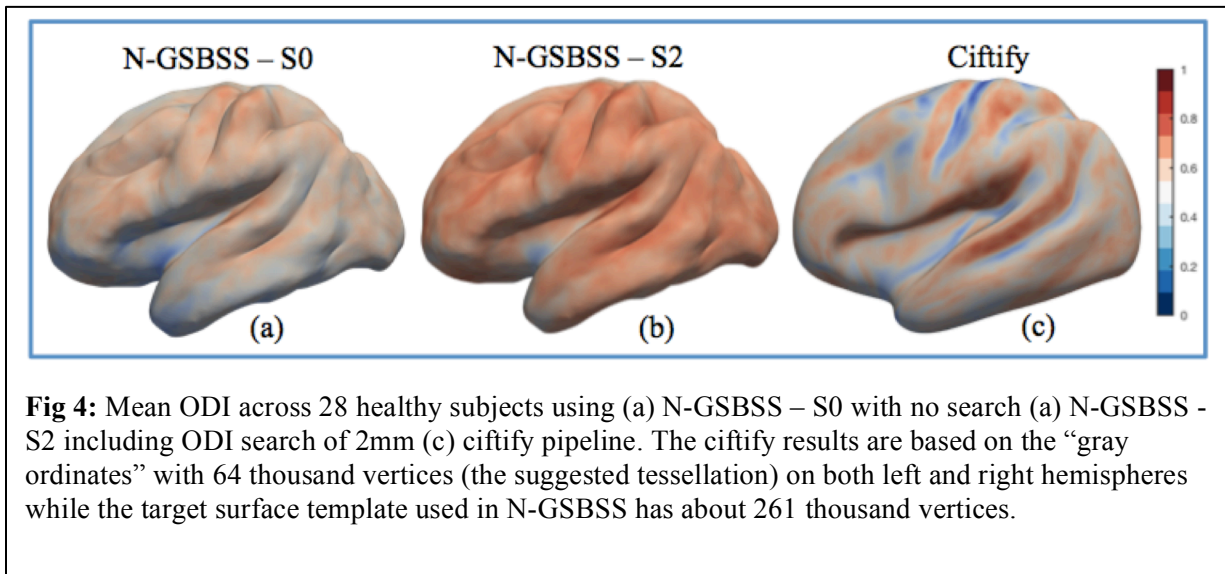


Fig 3: Flowchart of the N-GSBSS data processing for each subject. (1) The central surface is reconstructed via MaCRUISE (red) (2) and transformed to the MNI space (yellow) using ANTs volume registration. (3) These volumes are diffeomorphically registered to a single target surface. (4) Metrics of interest in other modalities are co-registered to corresponding anatomical T1-weighted image. (5) Cortical ODI search is performed using ODI and V_{iso} from NODDI metrics to search for higher ODI excluding V_{iso} within a given range (6) Data are processed for each modality (NODDI for diffusion microstructure and first level analysis for working memory tasks) to derive metrics of interest for cross-sectional analysis. (7) Metrics of interest are mapped onto the individual surface. (8) The mappings from shape correspondence are used to project intensity values of metrics of interest to the target surface (blue). (9) Vertex-wise spatial statistics on all projected data are performed on the target surface.

625
626
627



630
631

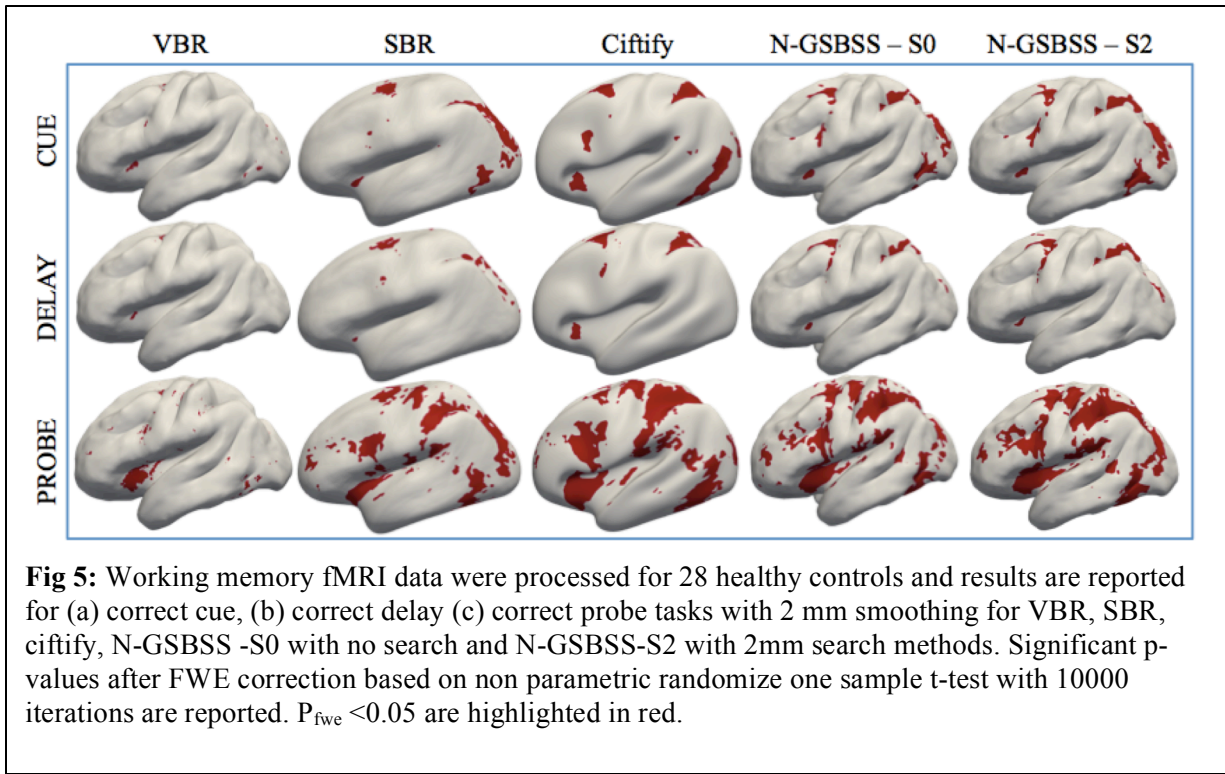


Fig 5: Working memory fMRI data were processed for 28 healthy controls and results are reported for (a) correct cue, (b) correct delay (c) correct probe tasks with 2 mm smoothing for VBR, SBR, ciftify, N-GBSS -S0 with no search and N-GBSS-S2 with 2mm search methods. Significant p-values after FWE correction based on non parametric randomize one sample t-test with 10000 iterations are reported. $P_{fwe} < 0.05$ are highlighted in red.

632
633

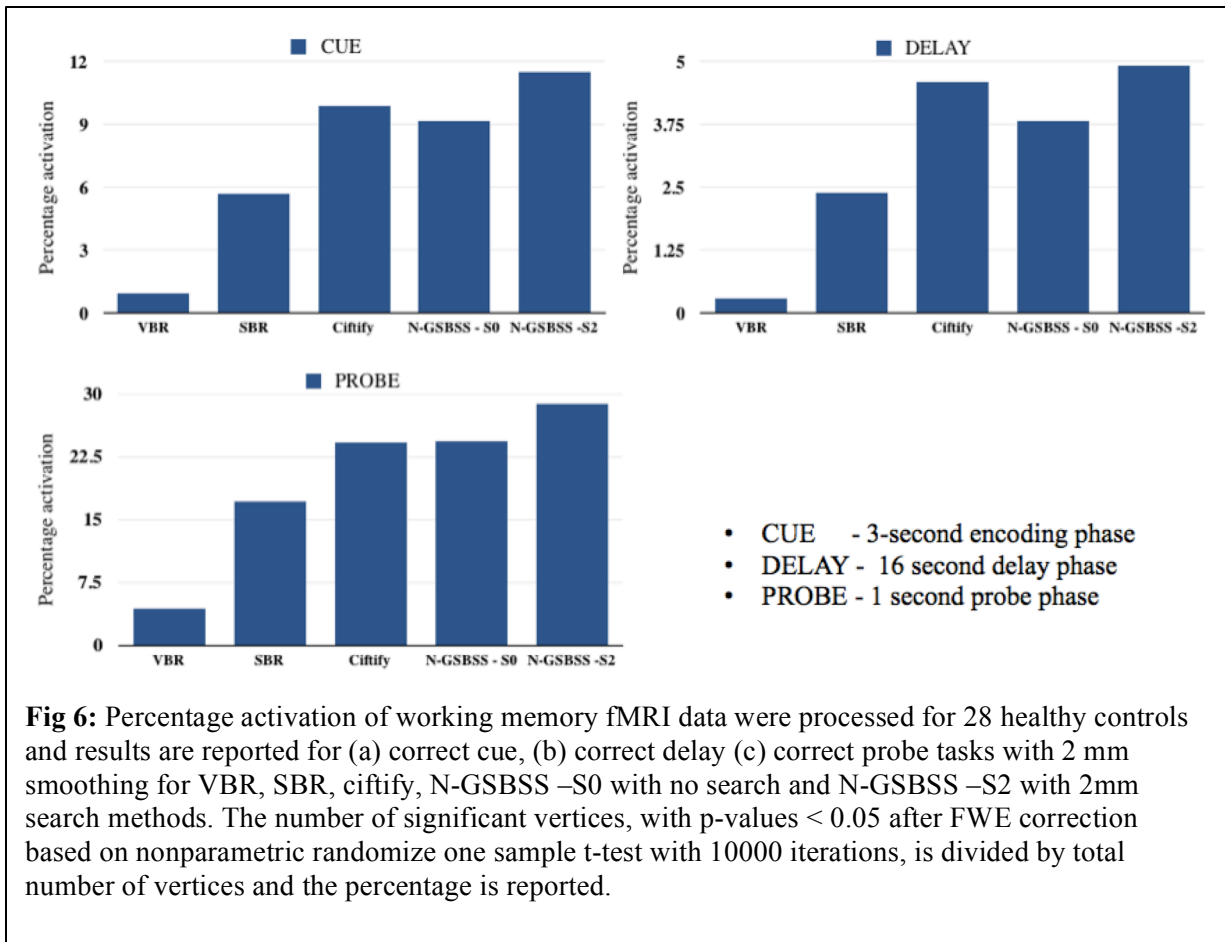


Fig 6: Percentage activation of working memory fMRI data were processed for 28 healthy controls and results are reported for (a) correct cue, (b) correct delay (c) correct probe tasks with 2 mm smoothing for VBR, SBR, ciftify, N-GSBSS –S0 with no search and N-GSBSS –S2 with 2mm search methods. The number of significant vertices, with p-values < 0.05 after FWE correction based on nonparametric randomize one sample t-test with 10000 iterations, is divided by total number of vertices and the percentage is reported.

634
635

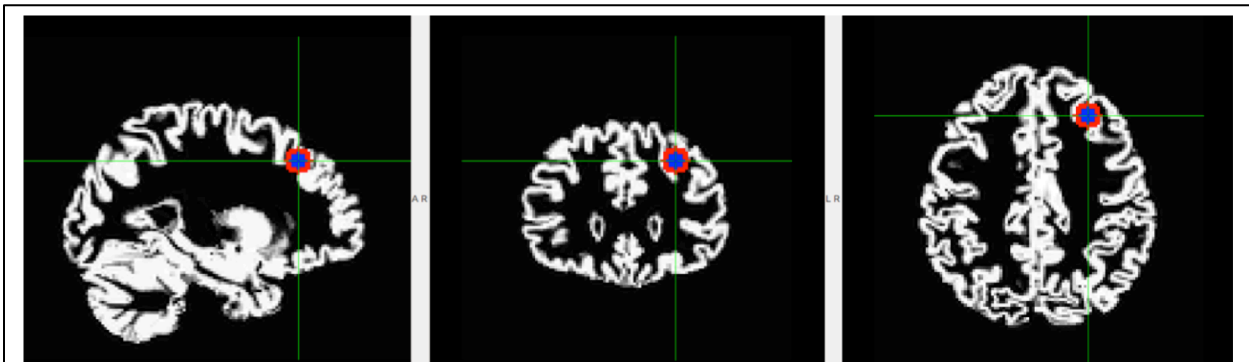


Fig 7: The gray matter probability map shows the simulated effect as an overlay mask of 5 mm (red) and 3 mm (dark blue) spheres.

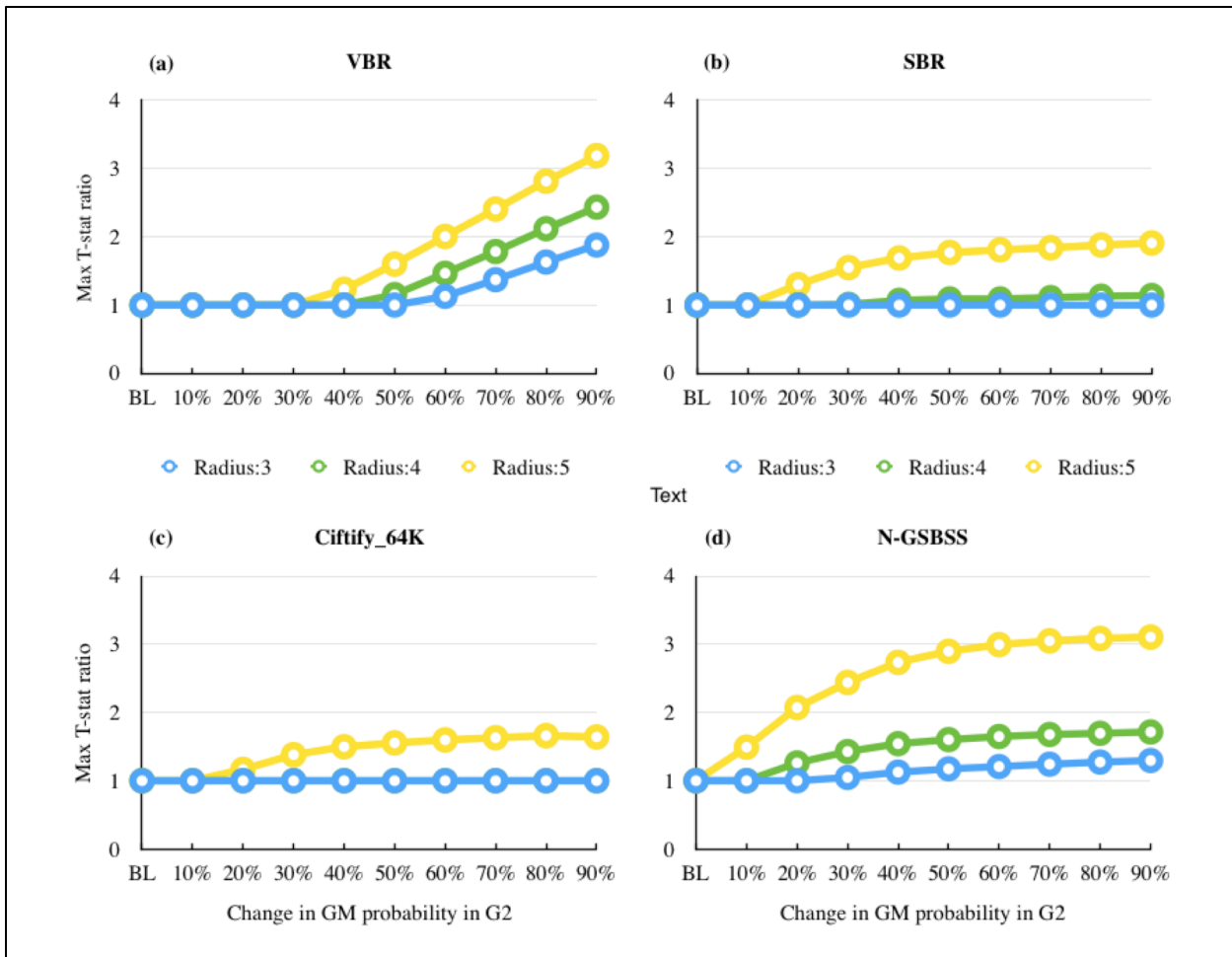


Fig 8: Quantitative results for statistical group differences over the change in lesion size from 3 to 5mm and percentage change from 10 percent to 90 percent. (a) Results from VBR analysis. (b) Results from FreeSurfer registration analysis. (c) Results from ciftify pipeline with default gray ordinates. (d) Results from GSBSS based analysis. Y-axis indicates maximum t-statistic ratio with respect to baseline. X-axis indicates the percentage change of GM probability in G2 with respect to original GM probability images in G2.